Fluid Structure and Motion Analysis from Multi-spectrum 2D Cloud Image Sequences

Abstract

In this paper we present a novel approach to estimate and analyze 3D fluid structure and motion of clouds from multi-spectrum 2D cloud image sequences. Accurate cloud-top structure and motion are very important for a host of meteorological and climate applications. However, due to the extremely complex nature of cloud fluid motion, classical nonrigid motion analysis methods will be insufficient to solve this particular problem. In this paper, two spectra of satellite cloud images are utilized. The high-resolution visible channel is first used to perform cloud tracking by using a recursive algorithm which integrates local motion analysis with a set of global fluid constraints which is defined according to the physical fluid dynamics. Then, the infrared channel (thermodynamic information) is incorporated to postprocess the cloud tracking results in order to capture the cloud density variations and small details of cloud fluidity. Experimental results on GOES (Geostationary Operational Environmental Satellite) cloud image sequences are presented in order to validate and evaluate both the effectiveness and robustness of our algorithm.

1 Introduction

The development of a robust automatic method of estimating cloud-top heights (structure) and winds (motion) from a sequence of meteorological satellite images is highly valuable. Accurate cloud heights and winds are very important for a number of meteorological and climate applications [6], such as cloud model verification [7], cloud-wind height assignment [13], and convective intensity estimation [19]. In particular, these information will enable us to obtain a better understanding of the structure and dynamics of hurricanes and severe thunderstorms. However, automatic analysis of cloud structure and motion is a very difficult problem due to the underlying non-linear phenomena of cloud formation and the extremely complex nature of cloud fluid motion. Classical nonrigid motion analysis algorithms usually assume local continuity and deal with shape changes of continuous surfaces. These algorithms will be insufficient in the case of fluid motion because there is usually no continuity constraint among neighboring elements which are free to move according to the underlying fluid dynamics. Some computational methods have been proposed to estimate fluid motion in recent years. However, most of them so far aimed at locating singular (or critical) points [18] [4] [14] [20], extracting vortex structures [21] [9], or estimating 2D fluid velocity fields [3] [12] in different image sequences such as meteorology images, oceanography images, and angiography images. Almost no work has been conducted to estimate both fluid structure and motion at the same time from 2D image sequences.

In particular, for the cloud tracking application, automatic cloud motion analysis under nonrigid deformations has been developed by Kambhamettu *et al.* [11] [10], Palaniappan *et al.* [16] [15], and Hasler *et al.* [8]. Kambhamettu *et al.* [11] used a *continuous motion model*, where individual cloud elements are assumed to undergo locally continuous deformation (i.e. the cloud surface patch can be smoothly stretched with local elements maintaining their neighborhood relationships) while Palaniappan *et al.* [16] [15] used a *semi-fluid model* which allows cloud surface patches to merge, split or cross over. However, their methods were based on 3D analysis because the changes in differential geometric properties of 3D cloud surface were utilized to perform cloud tracking. The 3D cloud data were obtained from stereo analysis, and/or approximating 2D intensity images for depth information. Authors in [1] estimated both the structure and 3D motion of hurricanes from a sequence of 2D satellite images. In their approach, affine motion model fitting within small cloud areas was first performed locally to get rough initial results, then global smoothing was applied to obtain hurricane top heights and motion. A structure and nonrigid motion analysis system, SMAS, was also implemented. However, due to the lack of a global dynamic description of the hurricane's fluid motion, their method suffered from the overconstrained smoothness assumption and had larger errors in the areas of hurricane eye and hurricane edge.

In this paper, we extend the work in [1] by exploit-

ing the fluid dynamics of cloud motion in order to relax the smoothness constraints. Two spectra of satellite cloud images are utilized. The high-resolution visible channel (10 bits) is first used to perform cloud tracking by using a recursive algorithm which integrates local motion analysis with a set of global fluid constraints, defined according to the physical fluid dynamics. Then, the infrared channel (thermodynamic information) is incorporated to postprocess the cloud tracking results in order to capture the cloud density variations and small details of cloud fluidity. The rest of the paper is organized as follows. In Section 2, we briefly review the local cloud tracking in [1] based on the visible channel of cloud images. In Section 3, a set of global fluid constraints is defined according the underlying fluid dynamics and a recursive algorithm is devised to integrate the local cloud motion analysis and the global fluid constraints. Section 4 presents a postprocessing process by incorporating the thermodynamic information from the IR (infrared) channel. This stage captures the cloud density variations and small details of cloud fluidity. Experimental results on GOES cloud image sequences are reported in Section 5. Finally, conclusions and future work are presented in Section 6.

2 Local Cloud Tracking

Cloud motion is a special case of fluid motion and consists of very complex motion dynamics. In order to obtain accurate cloud-top structure and motion, especially to capture small fluid details, local tracking techniques are necessary. Authors in [1] segmented the clouds evenly into many small areas and performed local motion model fitting within each area. Essentially, this local technique assumed that each small region is undergoing similar motion according to the same nonrigid motion model when the area is small enough (e.g. 3×3 pixels).

Affine motion model was chosen as the local cloud motion model in [1]. It was pointed out that although the affine transformation can only model continuous deformations, it is a good approximation for small local cloud motion[1]. In this paper, we derive the relationship between affine motion model and fluid dynamics in order to present affine's physical meaning for cloud fluid motion, presented in Appendix A.

Let us now briefly review the formulation of local cloud tracking with affine motion model in [1]. With the affine motion model, we have

$$\mathbf{P}^{i+1} = \mathbf{M}^i \mathbf{P}^i + \mathbf{D}^i, \tag{1}$$

where $\mathbf{P}^i(x^i, y^i, z^i)$ is a point in the frame i, $\mathbf{M}^i$ is an affine transformation matrix and $\mathbf{D}^i$ is a translation vector,

$$\mathbf{M}^i = \begin{pmatrix} {a_1}^i & {b_1}^i & {c_1}^i \\ {a_2}^i & {b_2}^i & {c_2}^i \\ {a_3}^i & {b_3}^i & {c_3}^i \end{pmatrix}, \quad \mathbf{D}^i = \begin{pmatrix} {d_1}^i \\ {d_2}^i \\ {d_3}^i \end{pmatrix}. \tag{2}$$

For cloud images, it can be assumed that the motion between successive frames is under the same motion model because it was experimentally found that a small cloud region moves smoothly [16], i.e.

$$\mathbf{M}^i = \mathbf{M} = \begin{pmatrix} a_1 & b_1 & c_1 \\ a_2 & b_2 & c_2 \\ a_3 & b_3 & c_3 \end{pmatrix}, \quad \mathbf{D}^i = \mathbf{D} = \begin{pmatrix} d_1 \\ d_2 \\ d_3 \end{pmatrix}. \tag{3}$$

However, since the time gaps between successive cloud images may not be constant, an additional scaling factor δ_i is incorporated in order to compensate for possible temporal deviations,

$$\mathbf{P}^{i+1} = \delta_i(\mathbf{M}\mathbf{P}^i + \mathbf{D}). \tag{4}$$

Eq. 4 represents the constraint equation for tracking a point across a sequence of images using affine motion model.

Levenberg-Marquardt non-linear least-square method is utilized to solve Eq. 4. Image registration techniques (cross-correlation or optic flow) are first used to find three 2D correspondence candidates for each data points. Then, an EOF (error-of-fit) function can be defined by the sum of the minimal distance between the 2D correspondence candidates and the orthographic projection[2] of the hypothesized point obtained by Eq. 4:

$$EOF_{local1} = \sum_{i=1}^{m \text{ frames}} \sum_{j=1}^{n \text{ points}} \min\left({d_{i,j}}^1, {d_{i,j}}^2, {d_{i,j}}^3\right), \tag{5}$$

where

$${d_{i,j}}^k = \left\| \left(\delta_i \left(\mathbf{M}\mathbf{P}_{i,j} + \mathbf{D}\right)^T \mathbf{R}_{ort}\right)^T - {\mathbf{C}_{i,j}}^k \right\|, \; k = 1, 2, 3. \tag{6}$$

[1] Actually, if the segmented areas are very small, they can be treated as localized particles whose motion may violate the continuity assumption according to the fluid dynamics. For the motion within the localized particles, tracked by local analysis, we can assume that the continuity is preserved [16].

[2] We can consider cloud images as orthographic projections since the distance between the satellite and clouds is very high (approximately 30,000 Kilometers).

${\mathbf{C}_{i,j}}^k$ are the three 2D correspondence candidates for point $\mathbf{P}_{i,j}$ and $\mathbf{R}_{ort}$ is the orthographic projection matrix,

$$\mathbf{R}_{ort} = \begin{pmatrix} 1 & 0 \\ 0 & 1 \\ 0 & 0 \end{pmatrix}. \tag{7}$$

The use of multiple correspondence candidates actually gives more flexibility to the minimization process in order to track the highly complex and dynamic cloud motion. Also, since the GOES satellite cloud images have a stereo occurrence every 15 minutes, the depth unknown in the first frame can be eliminated by fixing them to the available stereo disparities. Please see [1] for more details.

3 Global Fluid Constraints

Since the local optimization scheme performs cloud tracking within each small area independently, it suffers from discontinuities across borders, as the recovered structure and motion may change a lot from one small area to the other. Also, with the absence of a global description of the cloud fluid motion, there may be heavy over-fitting involved in the local motion model optimization. Hence, some appropriate global constraints are necessary in order to limit possible nonrigid behaviors and regularize the locally-recovered cloud motion and structure. In this paper, a set of global fluid constraints is defined according to the physical fluid dynamics.

3.1 Fluid Velocity Field Function

An important assumption of fluid velocity field is that the fluid velocity components can be represented by a Taylor series expansions as

$$\mathbf{v}_t(\mathbf{P}) = (v_{tx}(\mathbf{P}), v_{ty}(\mathbf{P}), v_{tz}(\mathbf{P}))^T, \tag{8}$$

where

$$\begin{aligned} v_{tx}(\mathbf{P}) &= u_0 + u_1 x + u_2 y + u_3 z + u_4 x^2 + u_5 y^2 + u_6 z^2 + \\ &\quad u_7 xy + u_8 xz + u_9 yz + \cdots, \\ v_{ty}(\mathbf{P}) &= v_0 + v_1 x + v_2 y + v_3 z + v_4 x^2 + v_5 y^2 + v_6 z^2 + \\ &\quad v_7 xy + v_8 xz + v_9 yz + \cdots, \\ v_{tz}(\mathbf{P}) &= w_0 + w_1 x + w_2 y + w_3 z + w_4 x^2 + w_5 y^2 + w_6 z^2 + \\ &\quad w_7 xy + w_8 xz + w_9 yz + \cdots. \end{aligned} \tag{9}$$

Essentially, Eq. 9 assumes that the fluid velocity components are smoothly varying functions with continuous derivatives. Many researchers have used it in fluid flow modeling and visualization. Perry [17] used it to model fluid flow fields and Ford *et.al.* [5] used it for fluid flow image visualization.

In the cloud application, we found that second order Taylor series expansion is a good approximation to the cloud velocity field. Hence, the locally tracked 3D cloud velocity can be globally constrained by three second order Taylor series expansions. A global velocity force can be defined as

$$E_v = \sum_{i=1}^{m \text{ frames}} \sum_{j=1}^{n \text{ points}} \left\| \text{diag}\left(\left(\mathbf{v}_{i,j} - \mathbf{v}_t^i(\mathbf{P}_{i,j}) \right) \boldsymbol{\lambda} \right) \right\|, \tag{10}$$

where

$$\mathbf{v}_{i,j} = \delta_i(\mathbf{M}\mathbf{P}_{i,j} + \mathbf{D}) - \mathbf{P}_{i,j}, \tag{11}$$

$\mathbf{v}_t^i$ is the velocity field function defined by second order Taylor series expansion for frame i and $\boldsymbol{\lambda} = (\lambda_1, \lambda_2, \lambda_3)^T$ are positive weights.

3.2 Fluid Dynamic Constraints

Besides the fluid velocity field function, the dynamics of fluid flows are further governed by three fundamental laws: the mass conservation law, Newton's second law of motion commonly known as Navier-Stokes equations in fluid mechanics, and the energy conservation law. In this application, since only kinematic information is available, we can use the mass conservation law to define a set of cloud fluid dynamic constraints. The law of conservation of mass is that the net flux of mass entering an infinitesimal control volume is equal to rate of change of the mass of the element. For homogeneous incompressible fluid, it is the divergence-free condition,

$$\nabla \cdot \mathbf{v} = \frac{\partial v_x}{\partial x} + \frac{\partial v_y}{\partial y} + \frac{\partial v_z}{\partial z} = 0. \tag{12}$$

Since the cloud velocity components can be represented by second order Taylor series expansion, the following constraint can be obtained after the mass conservation law is applied,

$$\begin{aligned} \nabla \cdot \mathbf{v}(\mathbf{P}) &= u_1 + 2u_4 x + u_7 y + u_8 z + v_2 + 2v_5 y + \\ &\quad v_7 x + v_9 z + w_3 + 2w_6 z + w_8 x + w_9 y \\ &= (u_1 + v_2 + w_3) + (2u_4 + v_7 + w_8)x + \\ &\quad (2v_5 + u_7 + w_9)y + (2w_6 + u_8 + v_9)z \\ &= 0. \end{aligned} \tag{13}$$

Eq. 13 actually provides a global fluid dynamic constraint for the 3D cloud motion tracking.

3.3 Integrating Local Cloud Tracking with Global Fluid Constrains

Having defined the global fluid constraints, the remaining problem is to integrate local cloud tracking and global fluid constraints together. However, all the coefficients in the defined global constraints (coefficients in Eq. 9) are unknown initially. In order to obtain the coefficient values which well describe the global cloud fluid motion, a recursive algorithm is devised in this paper.

First, the initial results for each small area without global constraints can be obtained by minimizing Eq. 5 locally. While the initial results may have a lot of noise, they can still be used to fit all the thirty coefficients in the velocity field functions (second order Tayler series expansion) for all the frames. Levenberg-Marquardt method is employed and the EOF function for fitting the velocity field functions in frame i can be simply defined as

$$EOF^i_{global1} = \sum_{j=1}^{N \text{ points}} \left\| \mathbf{v'}_{i,j} - \mathbf{v}^i_t(\mathbf{P}_{i,j}) \right\|, \qquad (14)$$

where $\mathbf{v}'_{i,j}$ is point j's velocity vector in frame i computed from the initial results. In addition, we want to include the fluid divergence-free condition (Eq. 12) into the fitting procedure, which can be done by rewriting Eq. 14 as the following,

$$EOF^i_{global2} = \sum_{j=1}^{N \text{ points}} \left(\left\| \mathbf{v'}_{i,j} - \mathbf{v}^i_t(\mathbf{P}_{i,j}) \right\| + \beta \left\| (\nabla \cdot \mathbf{v}^i_t(\mathbf{P}_{i,j}) \right\| \right), \qquad (15)$$

where β is a positive constant.

Second, after all the coefficients in Eq. 9 are fitted for all the frames, the global constraints can be easily incorporated into the local nonrigid motion model optimization by adding the velocity force to Eq. 5,

$$EOF_{local2} = \sum_{i=1}^{m \text{ frames}} \sum_{j=1}^{n \text{ points}} \min \left(d_{i,j}{}^1, d_{i,j}{}^2, d_{i,j}{}^3 \right) + E_v. \qquad (16)$$

Clearly, the new defined local EOF function (Eq. 16) contains both local and global information. More regularized results can be obtained by performing optimization on each small cloud area again by using Eq. 16. In this paper, the above procedure is performed recursively and the complete recursive algorithm is given in Algorithm 1.

Intuitively, Algorithm 1 retrieves useful information under proper constraints from current rough results and then uses the information as global constraints for the next iteration's optimization. A solid theoretical study of the convergence properties of the recursive algorithm is yet to be made, but our experimental results on GOES cloud image sequences presented in Section 5 show that the algorithm works very well for the particular cloud application and the desired convergence is achieved.

Algorithm 1: A Recursive Algorithm for Cloud Structure and Motion Tracking.

begin
  for $i := 1$ **to** n Areas **step** 1 **do**
    minimize Eq. 5 (without global constraints)
    to get initial results for small cloud area i;
  choose arbitrary initial **s** of large magnitude;
  while $\|\mathbf{s}\|$ is greater than some threshold **do**
    compute $\mathbf{v}'$ from the current results;
    for $i := 1$ **to** m Frames **step** 1 **do**
      minimize Eq. 15 to fit $\mathbf{v}^i_t(\mathbf{P})$ to $\mathbf{v}'$;
    for $i := 1$ **to** n Areas **step** 1 **do**
      minimize Eq. 16 (with global constraints)
      to get a new set of results for small
      cloud area i;
    calculate the difference **s** between the current results and the previous results;
end

4 Postprocessing with IR Information

In Eq. 12, it is assumed that clouds are homogeneous fluid, which means that there is no density variations over the entire clouds. However, this assumption fails in many highly dynamic cloud areas such as hurricane eyes and hurricane edges. In this paper, the thermodynamic information from the IR channel is utilized to postprocess and refine cloud tracking results in order to track the clouds more accurately for the cloud areas with density variations.

According to the mass conservation law, if the density variations are taken into account, we have

$$\frac{\partial \rho}{\partial t} + \mathbf{v} \cdot \nabla \rho + \rho \nabla \cdot \mathbf{v} = 0, \qquad (17)$$

where ρ is the fluid density. Obviously, for homogeneous fluid (ρ is a constant), Eq. 17 can be easily reduced to Eq. 12. It is clear that the density information is critical in order to incorporate Eq. 17 into the cloud tracking procedures. However, the cloud density is unknown. In fluid mechanics, it was pointed out that the density of saturated liquid varies considerably with the thermodynamic information for most

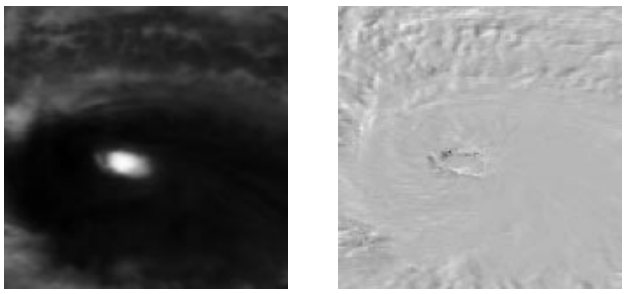

(a) (b)

Figure 1: (a): a sample cloud IR image from the GOES IR channel; (b): DI/Dt field.

substances, i.e. the density of fluid decreases as its temperature increases. Based on this observation, we assume that the cloud density is approximately inversely proportional to the cloud IR information (Note that IR is proportional to the temperature) in our particular cloud application, i.e.

$$\rho = \frac{K}{I}, \tag{18}$$

where K is a constant factor and I denote the cloud IR value. Although the fluid density may also change according to the pressure, especially in the region of critical points, we experimentally found that this assumption works very well and yield promising results.

Substitute Eq. 18 into Eq. 17, we have

$$\frac{\partial I}{\partial t} + \mathbf{v} \cdot \nabla I - I \nabla \cdot \mathbf{v} = 0, \tag{19}$$

where the first two terms can be designated by DI/Dt in the sense that it represents the rate of change in cloud temperature. Fig. 1 shows a sample cloud IR image and its DI/Dt field. Actually, Eq. 19 relaxes the fluid dynamic constraint defined in Eq. 13 at the cloud areas with density variations. Intuitively, one would like to simply replace 13 with Eq. 19 in the global cloud fluid constraints. However, our experimental results show that this step makes very trivial improvement to the cloud tracking results. The reason is that since most parts of the clouds have minor density variations, they will overwhelm the cloud areas with large density variations when fitting the global fluid velocity field functions. In order to deal with this problem, we postprocess the results from Algorithm 1 according to Eq. 19 within each small area individually. Since Eq. 19 is not incorporated into the global fluid velocity field functions, local density variations can be well captured. The whole postprocessing procedure is shown in Algorithm 2. Our experimental results show that this procedure is very effective and significantly reduces the tracking errors in highly dynamic cloud areas.

Algorithm 2: Postprocessing Cloud Structure and Motion Tracking Results with IR information.

begin
  perform cloud structure and motion tracking by using Algorithm 1 to get a set of results $\mathbf{v}$;
  calculate DI/Dt field from the IR information and the results $\mathbf{v}$;
  for $i := 1$ **to** n Areas **step** 1 **do**
    minimize Eq. 16 with previous results $\mathbf{v}$ as initial guesses and Eq. 19 as an additional constraint;
end

5 Experimental Results

Our algorithm has been extensively tested on the GOES image sequences of hurricane Luis which include 490 frames starting from 09-06-95 at 1023 UTC to 09-06-95 at 2226 UTC, provided by NASA-Goddard. Fig. 2 shows some sample input images. In this paper, in order to illustrate the improvement of our algorithm over [1], we present the results for the same cloud image sequence as in [1] (from 1621 UTC to 1634 UTC). Seven iterations were performed for this sequence by using the recursive algorithm. Fig. 3 shows the recovered cloud structure for the last frame (1634 UTC). In order to present the recovered cloud motion, we visualize the cloud motion in $x-y$ plane and in z direction separately. In fact, due to the orthographic projection in the cloud images, the recovery of z direction's motion is very important. Fig. 4 shows the recovered cloud motion which is projected to the $x-y$ plane and Fig. 5 illustrates the recovered z direction's motion (v_z) at every step in order to show the path taken by our algorithm. Obviously, the initially recovered z motion has a lot of noise. However, after the global fluid constraints were applied, the recovered z motion were improved and regularized. Fig. 5 shows that the final recovered cloud motion has higher v_z in hurricane eye and lower v_z in hurricane body, which is a regular phenomena for mature hurricanes [2]. When examining the recovered cloud motion closely, it can be noted that the fluid analysis enabled our algorithm to recover different kinds of nonrigid motion locally, including cloud surface expansion, contraction and also fluid phenomena such

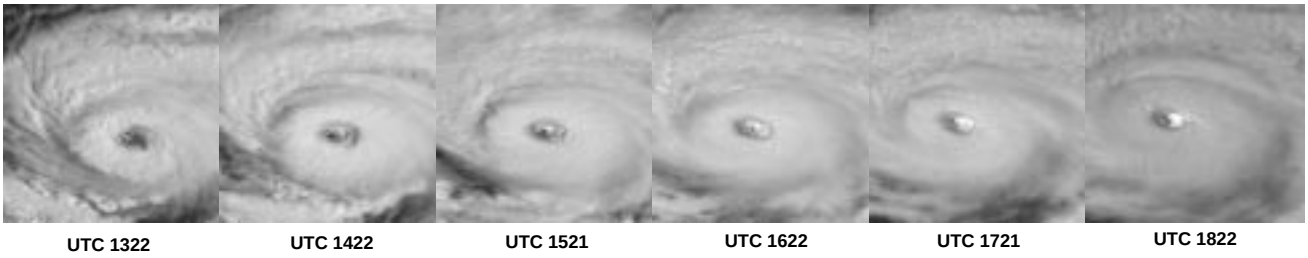

Figure 2: Sample satellite images of hurricane Luis.

Area	*Mean Error without Postprocessing*	*Mean Error with Postprocessing*
Hurricane Eye	1.037744	1.018575
Hurricane Body	0.707002	0.674495
Hurricane Edge	1.199529	0.816795

Table 1: Comparison of the results without and with the postprocessing step.

as cloud surface merging, splitting, crossing over and multi-layer motion, which are impossible in the results without multi-spectral fluid constraints. Movie clip 367-1.mpg presents the recovered cloud structure and motion through animation. This movie includes four parts. The first part shows a sample input cloud image sequence and the second part closely looks at the input images in order to show the presence of fluidity in cloud motion. The third part shows the recovered dense structure for the entire cloud while the last part shows some recovered fluid motion details.

In order to verify the results, we compared our estimated structure against the automatic stereo disparities[3] at the last frame (1634 UTC) because 1634 UTC is the only frame (from 1622 UTC to 1634 UTC) at which the disparities are available. In addition, we did this comparison at every iteration step in order to further evaluate the convergence and stability of our algorithm. Fig. 6 illustrates the change of the mean errors at different hurricane areas over several iterations. Note that although the initial mean errors are very large (about 2.5), they decrease very quickly after the global constraints are applied. Stable mean errors are achieved at the seventh iteration. Also, the

[3]The cloud disparities were provided by NASA-Goddard and have been validated in practical meteorological and climate applications.

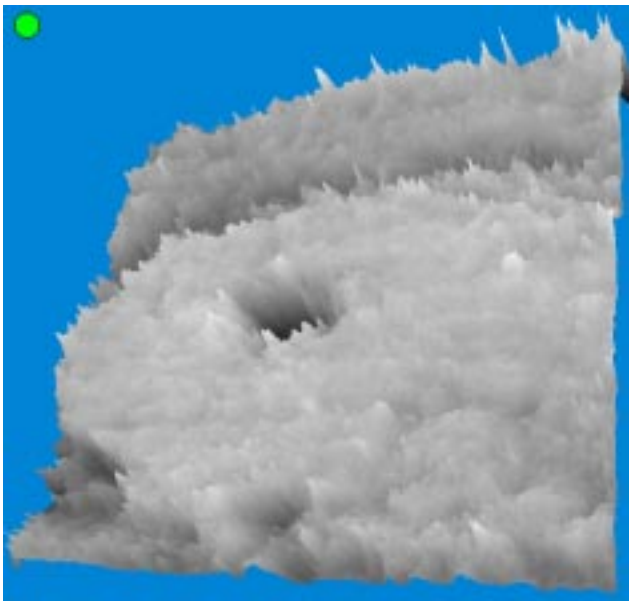

Figure 3: Recovered dense cloud heights at 1634 UTC.

postprocessing step significantly reduces the error in the area of hurricane edge because the hurricane edge has more density variations. Table 1 shows the mean errors of the results with and without postprocessing step. As can be seen, postprocessing introduces very trivial improvement in the area of hurricane eye, contradicting to our expectations. A possible explanation for this is that since the hurricane eye is the place where most of the energy conversion occurs [2], the fluid motion within this area is too complex and dynamic to be tracked by local affine motion model. More complex motion model will be investigated for the eye area in the future. Except the hurricane eye, the errors for our estimated results are very small (0.6 to 0.8).

6 Conclusions and Future Work

We have described an automatic method to estimate both fluid structure and motion from multi-

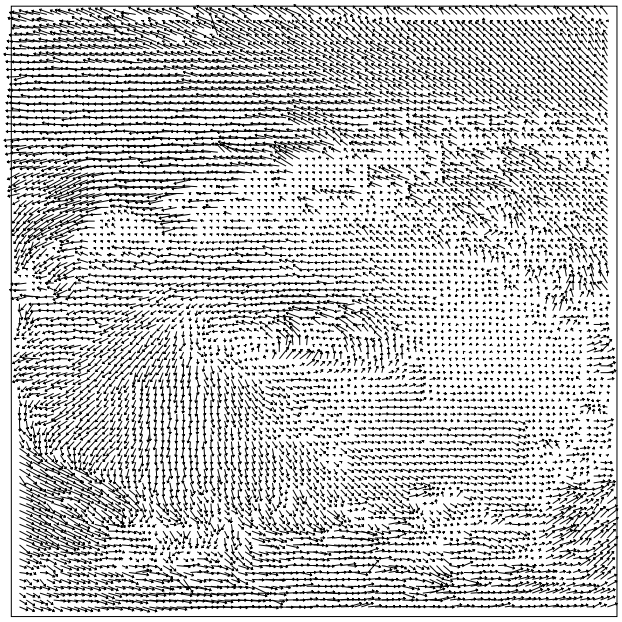

Figure 4: Recovered cloud motion which is projected to the $x-y$ plane.

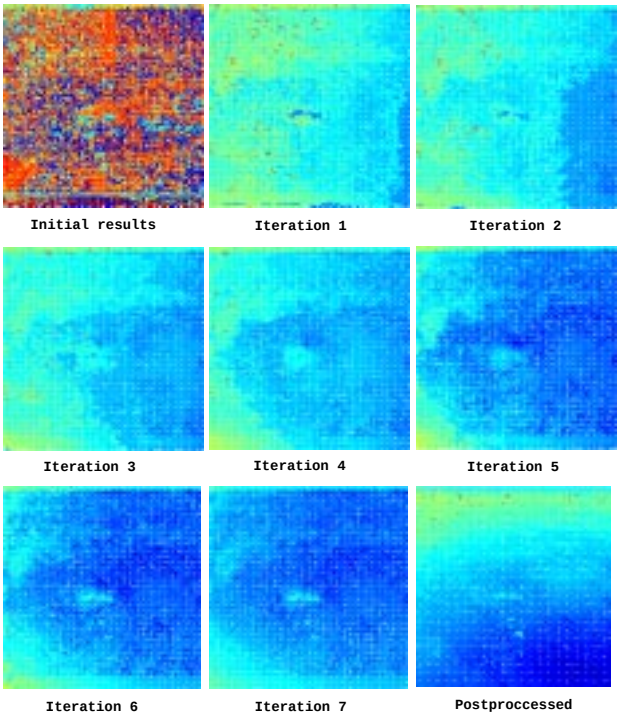

Figure 5: Recovered cloud motion in z direction (v_z) at every step.

spectrum satellite cloud image sequences. A recursive algorithm is proposed to integrate local cloud tracking with a set global fluid constraints which is defined according to the underlying fluid dynamics. In addition, the utilization of IR information enabled us to capture the cloud density variations. Encouraging results on GOES satellite hurricane images confirm both the robustness and the effectiveness of our method. We believe that our methodology can be extended to other fluid data such as oceanography images (e.g. sea, ice), and angiography images (e.g. blood flow). The future directions include developing complex local motion models for the hurricane eye area, cloud motion segmentation, and cloud model visualization.

Acknowledgments

Research funding was provided by the National Science Foundation.

Appendix A: Affine Motion Model and Cloud Fluid Dynamics

For incompressible flows for which the variation of fluid viscosity can be considered negligible, the Navier-Stokes equations describes the flow fluid dynamics as the following,

$$\rho\frac{Dv_x}{Dt} = -\frac{\partial p}{\partial x} + \mu\left(\frac{\partial^2 v_x}{\partial x^2} + \frac{\partial^2 v_x}{\partial y^2} + \frac{\partial^2 v_x}{\partial z^2}\right) + \rho g_x,$$

$$\rho\frac{Dv_y}{Dt} = -\frac{\partial p}{\partial y} + \mu\left(\frac{\partial^2 v_y}{\partial x^2} + \frac{\partial^2 v_y}{\partial y^2} + \frac{\partial^2 v_y}{\partial z^2}\right) + \rho g_y,$$

$$\rho\frac{Dv_z}{Dt} = -\frac{\partial p}{\partial z} + \mu\left(\frac{\partial^2 v_z}{\partial x^2} + \frac{\partial^2 v_z}{\partial y^2} + \frac{\partial^2 v_z}{\partial z^2}\right) + \rho g_z. \tag{20}$$

These equations can be easily put into the compact vector form as

$$\rho\frac{D\mathbf{v}}{Dt} = -\nabla\cdot p + \mu\nabla^2\cdot\mathbf{v} + \rho\mathbf{g}. \tag{21}$$

where p is the pressure, ρ is the fluid density, μ is the viscosity of the fluid, $\mathbf{v}$ is the velocity vector, and $\mathbf{g}$ is the gravity vector.

Considering affine motion model, let the time gap between two successive frames be the unit time, the velocity vector can be easily obtained by

$$\mathbf{v} = \mathbf{MP} + \mathbf{D} - \mathbf{P} = (\mathbf{M}-\mathbf{I})\mathbf{P} + \mathbf{D}. \tag{22}$$

Hence, we have

$$\frac{D\mathbf{v}}{Dt} = \frac{D(\mathbf{M}-\mathbf{I})\mathbf{P}}{Dt} + \frac{D\mathbf{D}}{Dt} = (\mathbf{M}-\mathbf{I})\mathbf{v}, \tag{23}$$

and

$$\nabla^2\cdot\mathbf{v} = \nabla^2\cdot((\mathbf{M}-\mathbf{I})\mathbf{P} + \mathbf{D}) = 0. \tag{24}$$

Substituting Eq. 23 and Eq. 24 to Eq. 21, we have

$$\rho(\mathbf{M}-\mathbf{I})\mathbf{v} = -\nabla\cdot p + \rho\mathbf{g}. \tag{25}$$

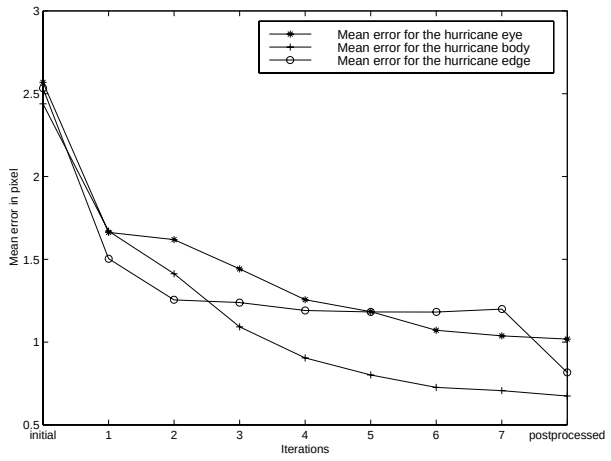

Figure 6: The mean errors of different hurricane areas when comparing our estimated structure against the disparities from stereo analysis.

For cloud motion, since cloud is far away from the earth surface, gravity vector $\mathbf{g}$ is almost negligible. Thus, the following equation can be obtained,

$$\nabla \cdot p = -\rho(\mathbf{M} - \mathbf{I})\mathbf{v}. \tag{26}$$

Eq. 26 presents the relationship between affine motion model and the local cloud fluid dynamics. From the fluid dynamics point of view, the use of affine motion model to simulate local cloud motion is just assuming that the divergence of pressure p in local cloud area is a linear combination of cloud velocity components.

References

[1] Extracting nonrigid motion and 3D structure of hurricanes from satellite image sequences without correspondence. *IEEE Conference on Computer Vision and Pattern Recognition*, pages II–280–285, 1999.

[2] Jorgensen D.P. Mesoscale and convective-scale characteristics of mature hurricanes: Part I. general observations by research aircraft. *J. Atmos. Sci.*, 41:1268–1285, 1984.

[3] E.M. Emin and P. Perez. Fluid motion recovery by coupling dense and parametric vector fields. In *ICCV99*, pages 620–625, 1999.

[4] R.M. Ford. Critical-point detection in fluid flow images using dynamical system properties. *PR*, 30(12):1991–2000, December 1997.

[5] R.M. Ford and R.N. Strickland. Representing and visualizing fluid-flow images and velocimetry data by nonlinear dynamical-systems. *GMIP*, 57(6):462–482, November 1995.

[6] A. F. Hasler. Stereoscopic measurements. In P. K. Rao, S. J. Holms, R. K. Anderson, J. Winston, and P. Lehr, editors, *Weather Satellites: Systems, Data and Environmental Applications, Section VII-3*, pages 231–239. Amer. Meteor. Soc., Boston, MA, 1990.

[7] A. F. Hasler and K. R. Morris. Hurricane structure and wind fields from stereoscopic and infrared satellite observations and radar data. *J. Climate Appl. Meteor.*, 25:709–727, 1986.

[8] A. F. Hasler, K. Palaniappan, C. Kambhamettu, P. Black, E. Uhlhorn, and D. Chesters. High resolution wind fields within the inner-core and eye of the a mature tropical cyclone using a long series of geos one-minute images and a massively parallel computer. *Bulletin of the American, Meteorological Society*, 1998.

[9] P.C. Hu and R.N. Strickland. Detection of vortices in flow iamges using the wavelet transform. In *ICIP99*, page 26PP1, 1999.

[10] C. Kambhamettu, K. Palaniappan, and A. F. Hasler. Coupled, multi-resolution stereo and motion analysis. *IEEE International Symposium on Computer Vision*, pages 43–48, November 1995.

[11] Chandra Kambhamettu, K. Palaniappan, and A. Frederick Hasler. Automated cloud-drift winds from goes-8/9. *SPIE - International Symposium on Optical Science, Engineering and Instrumentation*, August, 1996.

[12] M. Maurizot, P. Bouthemy, and B. Delyon. 2d fluid motion analysis from a single image. In *CVPR98*, pages 184–191, 1998.

[13] P. Minnis, P. W. Heck, and E. F. Harrison. The 27-28 october 1986 fire ifo cirrus case study: Cloud parameter fields derived from satellite data. *Monthly Weather Review*, 118:2426–2447, 1990.

[14] H. Nogawa, Y. Nakajima, Y. Sato, and S. Tamura. Acquisition of symbolic description from flow-fields: A new approach based on a fluid model. *PAMI*, 19(1):58–63, January 1997.

[15] K. Palaniappan, M. Faisal, C. Kambhamettu, and A. F. Hasler. Implementation of an automatic semi-fluid motion analysis algorithm on a massively parallel computer. *IEEE International Parallel Processing Symposium*, pages 864–872, 1996.

[16] K. Palaniappan, Chandra Kambhamettu, A. Frederick Hasler, and Dmitry B. Goldgof. Structure and semi-fluid motion analysis of stereoscopic satellite images for cloud tracking. *Proceedings of the International Conference on Computer Vision*, pages 659–665, 1995.

[17] A. E. Perry and M. S. Chong. A description of eddying motions and flow patterns using critical point concepts. *Ann. Rev. Fluid Mech.*, 19:125–155, 1987.

[18] A.R. Rao and R.C. Jain. Computerized flow field analysis: Oriented texture fields. *PAMI*, 14(7):693–709, July 1992.

[19] E. Rodgers, R. Mack, and A. F. Hasler. A satellite stereoscopic technique to estimate tropical cyclone intensity. *Monthly Weather Review*, 111:1599–1610, 1983.

[20] C.F. Shu and R.C. Jain. Vector field analysis for oriented patterns. *PAMI*, 16(9):946–950, September 1994.

[21] J.L. Zhong, T.S. Huang, and R.J. Adrian. Extracting 3d vortices in turbulent fluid-flow. *PAMI*, 20(2):193–199, February 1998.